Deployment and Implementation Strategies for Massive MIMO in 5G

Berthold Panzner*, Wolfgang Zirwas*, Stefan Dierks†
Mads Lauridsen‡, Preben Mogensen‡, Kari Pajukoski§ and Deshan Miao¶
* Nokia Networks, Radio Systems Research, Munich/Germany
† Technische Universität München, Institute for Communications Engineering, Munich/Germany
‡ Aalborg University, Wireless Communication Networks, Aalborg/Denmark
§ Nokia Networks, Radio Systems Research, Oulu/Finland
¶ Nokia Networks, Radio Systems Research, Beijing/China

***Abstract*—Massive MIMO has emerged as one technology enabler for the next generation mobile communications 5G. The gains promised by massive MIMO are augured to overcome the capacity crunch in today's mobile networks and to pave the way for the ambitious targets of 5G. The challenge to realize massive MIMO for 5G is a successful and cost-efficient integration in the overall network concept. This work highlights deployment and implementation strategies for massive MIMO in the context of 5G indoor small cell scenarios. Different massive MIMO deployment scenarios are analyzed for a standard 3GPP indoor office scenario. In particular stand-alone MIMO at a single location, distributed MIMO without cooperation and network MIMO with full cooperation are investigated for varying array configurations. For the performance analysis of the different MIMO configurations the ratio of total transmit antennas to spatial streams is varied stepwise from equality to a factor of ten. For implementation of massive MIMO in 5G networks trends in beamforming techniques, mutually coupled subarrays, over the calibration procedure and estimated ADC performance in 2020 time-frame are discussed. Based on the debate the paper indicates how to integrate large-scale arrays in future 5G networks.**

I. Introduction

With the advent of the global mobile communication standard 4G issued by the Third Generation Partnership Project (3GPP) as Long Term Evolution (LTE) in 2008 multiple-input multiple-output (MIMO) techniques have been included in the standard as prerequisite from the very beginning. In subsequent 4G releases MIMO has been steadily enhanced to support up to 8 spatial streams to a single terminal in downlink (SU-MIMO) as well as simultaneous downlink transmission to maximal 4 individual terminals (MU-MIMO). The seminal paper of [1] has created new attention to the topic, where a vast amount of base station antennas promises huge capacity gains compared to todays mobile communication systems. Since then massive MIMO (mMIMO) has become a dominant driver in the discussion for a successor of 4G.

The terminology *massive MIMO* is however not clearly defined. In some communities mMIMO defines any MIMO configuration beyond the highest MIMO mode in current LTE (at present 8x8), other communities refer mMIMO simply to large number of antennas at the base stations. A somewhat more precise way to define mMIMO is to relate it to the ratio of active users to antennas that serve those users. In Fig. 1 the aggregated throughput is plotted versus the ratio of terminals k over antennas N_T at the base station. If the number of users compared to number of base station antennas is low, all users in the cell can be served simultaneously without any penalty in user-specific throughput. If more users attach to the cell it reaches its maximum capacity, the optimal point where the maximal cell resources are distributed among all users. If the number of users further increases the network is forced to schedule users in an appropriate manner to fulfill fairness constraint, resembling a state of resource limitation. In the resource limited region a real network can not deliver requested resources to all users simultaneously due to non-optimal scheduling decisions and consequently the sum throughput decreases. Hence in this context mMIMO is understood as a vast over-provisioning of resources that do not depend on any scheduling or load balancing in multi-cell scenarios. Thus mMIMO presents a fundamental paradigm shift [2] to today's resource limited communication systems rather than a simple increase in number of base station antennas. The gains of this radical approach of mMIMO for 5G have been discussed in [3] and [4].

In the context of the demanding 5G targets [5] mMIMO is key to achieve peak data rates up to 10Gbit/s as illustrated in Fig. 2, visualizing the trade-off between the three fundamental radio resources (spectrum, modulation order, spatial streams). The color in Fig. 2 represents the required modulation order for a given bandwidth and given a number of parallel streams to yield 10Gbit/s peak rate over the air-interface (included a 30% overhead for control signaling). If we assume for exemple a 200MHz system bandwidth for 5G (cf. Tab. II) and 64-QAM at least 12 parallel MIMO streams are necessary to support 10Gbit/s peak rate. Instead of promoting the gains of mMIMO in general the authors provide in the following a vision on strategies how to realize and deploy mMIMO in a typical indoor 5G scenario.

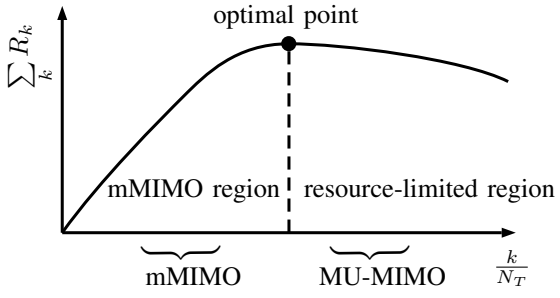

Fig. 1. Paradigm Shift of Massive MIMO

978-1-4799-7470-2/14/$31.00 ©2014 IEEE

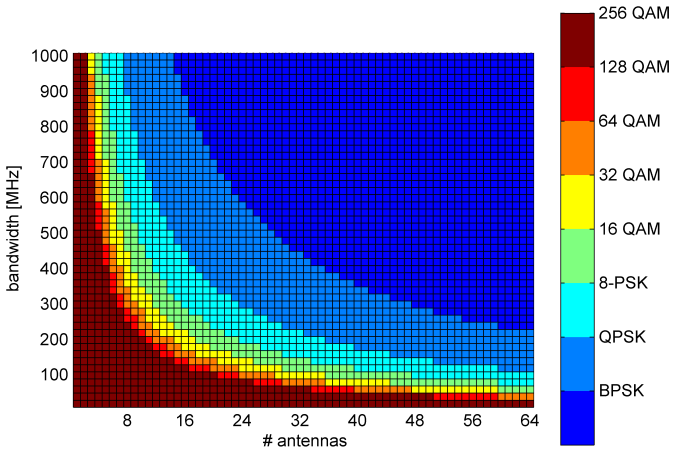

Fig. 2. Minimum required modulation order (bit/RE) for 10Gbit/s peak data rate (incl. 30% overhead) for varying number of antennas and bandwidth

II. Deployment Strategies

Most of the investigated mMIMO scenarios consider preferably wide area outdoor deployments [3]. However most of the mobile traffic is generated by indoor users [6].
In the following three indoor mMIMO deployments for the standard 3GPP two stripe office building [7] are analyzed: standalone massive MIMO at a single location (single mMIMO), distributed MIMO without cooperation (distributed mMIMO) and network MIMO with full cooperation (network mMIMO). The scenario layout is shown in Fig. 3. For all configurations rectangular arrays with inter-element spacing of $\lambda/2$ have been used, where the total number of transmit antennas compared to number of fixed users has been increased from factor 1 up to factor 10. The fading channel is generated by the 3D geometry based statistical channel model *QuaDRiGa* [9] based on the WINNER2 [8] indoor parameters listed in Tab. I.

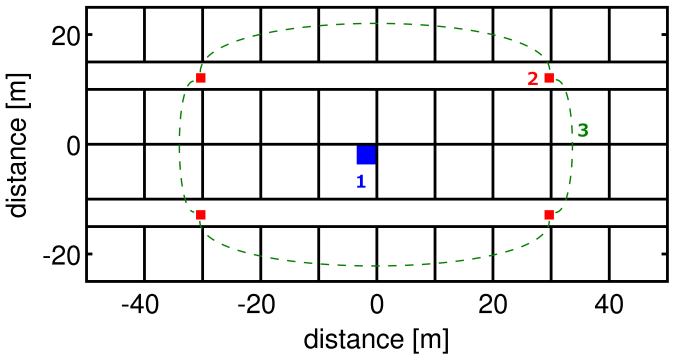

Fig. 3. 3GPP standard office scenario (blue: single massive MIMO, red: distributed MIMO without cooperation, green: network MIMO with cooperation)

TABLE I. WINNER2 [8] Indoor Channel Parameters

Model	Scenario	Cond.	Sym.	Value
A1	indoor office	LOS	α	18.7
			β	46.8
			χ_σ	3
		NLOS	α	36.8
			β	43.8
			χ_σ	4

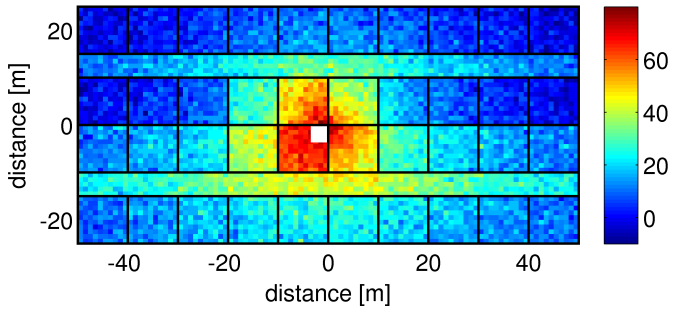

Fig. 4. Average SNR [dB] for single array (MRT to one single antenna UE with $N_T = 36$ total transmit antennas)

The path loss is evaluated as:

$$PL = \alpha + \beta \log_{10}\left(\frac{d}{1\text{m}}\right) + \gamma \log_{10}\left(\frac{f_c}{5\text{GHz}}\right) + W_l\,(n_W - 1) + \chi_\sigma \quad (1)$$

where d is the distance between the base station and an UE, α is the intercept point, β is the path loss slope, γ is the frequency dependent attenuation (here γ=20), χ_σ is the log-normal distributed shadow fading with standard deviation σ. There is an additional loss W_l due to wall penetration of n_W walls (here 12dB for heavy wall).
In Fig. 4 the SNR distribution achieved with maximum ratio transmission (MRT) for a single array and in Fig. 5 achieved with four cooperating arrays are illustrated for $N_T = 36$ total transmit antennas and a sum power power constraint. Obviously the SNR distribution for the deployment with a single array suffers from multiple wall penetration loss compared to the distributed deployment. However for the distributed array placement also higher capex, larger installation expenditure and in case of cooperation between the arrays the necessity of a powerful backhaul have to be considered for a fair comparison. For all three MIMO modes (single mMIMO, distributed mMIMO without cooperation, network mMIMO with full cooperation) zero-forcing precoding with a total transmit power constraint has been applied in a multi-user scenario with 20 single-antenna UEs. The optimal solution for sum rate maximization given a total power constraint is the pseudo-inverse using water filling as the power allocation scheme [10]. Here an equal power transmission to each UE has been chosen, whereas the distribution of the per-UE transmit power on the subcarriers is determined by the water filling solution. The cumulative distribution of the spectral efficiency (SE) for all 3 MIMO modes are plotted in Fig. 6 for varying

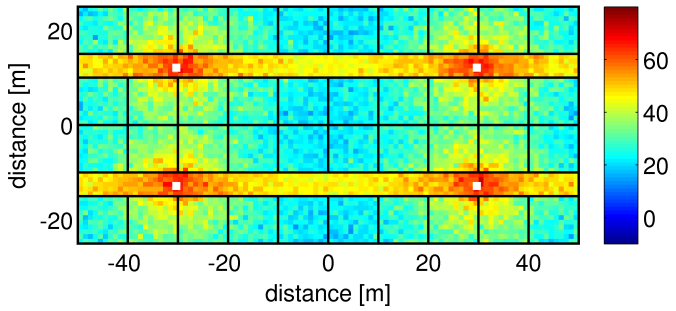

Fig. 5. Average SNR [dB] for cooperating arrays (MRT to one single antenna UE with $N_T = 36$ total transmit antennas)

TABLE II. 5G PHYSICAL LAYER SYSTEM PARAMETERS

Symbol	Parameter	Value
P_T	total transmit power	26dBm
f_c	carrier frequency	3.5GHz
BW	system bandwidth	200MHz
# FFT	FFT length	4096
f_s	clock rate	64×3.84 Mchip/s
Δf	subcarrier spacing	60kHz
n	eff. subcarrier	3200
TTI	frame length	250μs
T_s	symbol time	16.67μs
# symbols	symbols per frame	11data+3control
max(AMC)	highest modulation order	256 QAM

numbers of antennas at the base station. The 20 UEs have been dropped at 300 different positions with 10 channel realizations per drop. The spectral efficiency for all three MIMO modes is derived by the numerology in [11]. The maximal achievable spectral efficiency for 20 UEs according to the physical layer parameters listed in Tab. II is:

$$20\frac{\log_2(256)\text{bits}\cdot 3200\cdot 11}{250\mu\text{s}\cdot 200\text{MHz}} = 112.46\text{bit/s/Hz} \qquad (2)$$

In single mMIMO as well as network MIMO with full cooperation all users are served simultaneously. For the distributed MIMO without cooperation the UE connects to the array with the maximum average SNR and precoding is performed locally by that specific array while treating interference of other downlink transmissions as noise. In case more UEs connect to one array as there are transmit antennas, the UEs are scheduled with channel decomposition using capacity upperbound [12]. As seen in Fig. 6 single mMIMO (solid lines) results in the lowest SE, distributed MIMO without cooperation (dashed lines) gives significant SE gains over the single mMIMO case, whereas network MIMO with full cooperation (dotted lines) yield the highest SE. The fully loaded scenario ($N_T = N_{UE} = 20$) reveals the lowest SE compared to setups with higher number of antennas. If N_T is just increased slightly by 4 to 24 TX antennas the SE is doubled, thus for this deployment scenario a 20% increase in TX antennas above baseline configuration ($N_T = N_{UE}$) results in 100% capacity gain. Adding more antennas increases the performance though with decreasing gain per each additional antenna, e.g. a 1000% increase in TX antennas results in less than 1000% capacity

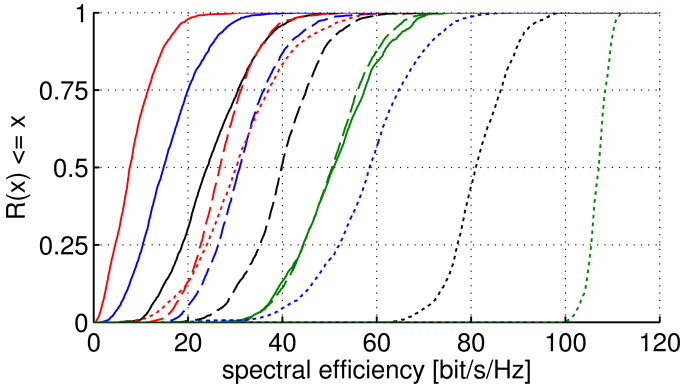

Fig. 6. CDF of SE for 20 UEs (red: $N_T = 20$, blue: $N_T = 24$, black: $N_T = 36$ and green: $N_T = 200$ total transmit antennas; solid: single mMIMO, dashed: distributed mMIMO, dotted: network mMIMO)

TABLE III. SPECTRAL EFFICIENCY PERCENTILES

MIMO MODE	N_T	Percentile [bit/s/Hz]		
		5%	50%	95%
Single Massive MIMO	20	1.8	7.7	17.8
	200	36.5	50.9	66.9
Distributed MIMO excl. cooperation	20	17.2	26.8	38.5
	200	36.7	50.6	64.1
Network MIMO incl. cooperation	20	15.0	30.3	49.5
	200	103.0	107.0	110.0

gain. In Fig. 6 distributed MIMO with 24 TX antennas results in a similar performance as network MIMO with only 20 TX antennas. Thus potential hardware savings due to less antennas have to be balanced with additional cost required for backhaul. Furthermore Fig. 6 reveals that for 20 TX antennas the difference between single mMIMO and distributed MIMO is threefold while for 200 TX antennas the difference between single mMIMO and distributed mMIMO is negligible. For a ratio of 10 of transmit antennas to UEs the SE cdf curve is approaching a step function, i.e. cell edge users (5%tile) and 95%tile users observe almost the same rate (cf. Tab. III). In summary the optimal deployment strategy is a scenario-dependent trade-off between various metrics.

III. IMPLEMENTATION STRATEGIES

A. Beamforming Architecture

The crucial point to realize real-world massive MIMO arrays is an extremely cost-effective transmitter architecture for the multitude of transmit antennas. Most efforts on mMIMO demonstrators concentrate on the integration of the TX/RX front-end directly onto the radiating element in order to create an active antenna system, where each individual array element is composed of a fully active TX/RX module. However a fully active antenna system still requires a fairly high amount of expensive components such as ADC/DAC, envelope tracking RF amplifiers, TX/RX switches, filters, etc. at each individual antenna element. Therefore hybrid beamforming concepts (see Fig. 7), a combination of digital and analog beamforming, have become popular for mMIMO. The digital beamforming part formulates baseband precoding, while the analog beamforming part conducts coarse RF beamforming. In large scale antenna systems hybrid beamforming concepts can provide cost-saving effects by reducing the number of ADC/DAC and digital baseband processing units while maintaining multi-user beamforming capabilities with a slightly reduced degree of freedom compared to the fully active transmit architecture. The hybrid beamforming concept naturally supports the subarray

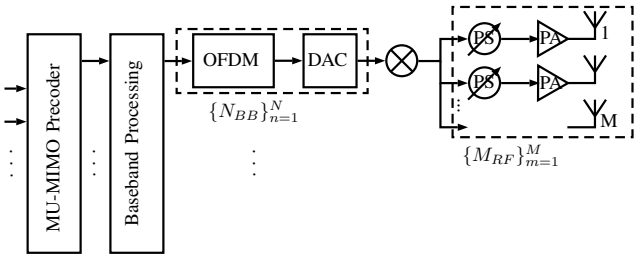

Fig. 7. Hybrid beamforming transmitter architecture (N number of digital baseband units, M number of RF units per subarray)

concept, where the total large scale antenna array is composed of smaller sub-arrays. Analog beamforming by the digitally controlled phase-shifters is performed per subarray, while digital precoding is performed over the complete set of subarrays. In the following we will discuss briefly scalable subarrays based on mutually coupled antennas, calibration issues for distributed mMIMO arrays and predicted ADC performance in 2020.

B. Mutually Coupled Subarrays

Evidently large scale antenna arrays will increase the physical dimension of the base station antenna, generating negative consequences on weight, wind load and visual impact. The majority of present mMIMO arrays are uniform arrangements of radiator elements on a planar or cylindrical surface. However the strict space constraints on antenna housing will force 5G large scale array design to exploit more advanced technologies such as antennas on flexible substrates or organic printed antennas to support a higher level of visually obscured integration in the natural surrounding of the users [13]. Whereas millimeter waves easily allow the accommodation of more antennas onto a given area the challenge for lower GHz frequency bands, like the classical mobile communication frequency bands around 2GHz, remains tough. One approach to utilize the restricted antenna space is to exploit mutual coupling for dense antenna placement. In this work a novel array configuration based on mutually coupled subarrays composed of four closely spaced elements is proposed to ease the placement of many antennas on a restricted area.
Mutual coupling, i.e. the electromagnetic interaction between very closely spaced antennas ($l < 0.1\lambda$) over the near field, is incorporated analytically by a mutual coupling matrix describing the inter-element interaction. In a three dimensional electromagnetic field simulator the subgroup composed of four tightly spaced radiating elements with inter-element spacing of 0.1λ has been arranged to an uniform array as illustrated in Fig. 8. The field simulator has revealed that the effects of mutual coupling result in different preferred far field directions for the individual radiators compared to the uncoupled case. That observation has first been noticed in a MIMO hardware demonstrator, where the tight spacing of the four movable antenna elements of a 4TX array has not caused any reduction in MIMO rank and total system throughput for the four streams. This remarkable result has been verified by the pattern measurements and published in [14].
In order to assess the impact of mutually coupled subarrays on system level performance, a ray tracing simulation of the array configuration shown in Fig. 8 has been performed based on the model of the Nokia campus in Munich. In this multiuser scenario 6 UEs have been placed across the campus map and the effective channels derived by the ray-tracing tool have been analyzed. The singular value decomposition of the aggregated MIMO channel has been performed for all 6 users over 256 subcarriers with 60kHz spacing. The condition number of the channel matrix, i.e. the ratio of the singular values expressing how well the channel is suitable for spatial multiplexing, for a group of 6 users varies between 6 (best case) and 24 (worst case, condition number in linear scale) over all subcarriers. Thus in this ray-tracing analysis for evaluation of system level performance it has been demonstrated that arrays of mutually coupled subgroups lead to decorrelated multi-user MIMO channels [15].
The proposed subarray configuration based on mutually coupled antenna elements provides a space-saving and scalable concept for large scale arrays that is especially suitable for hybrid beamforming, where precoding can be performed on top.

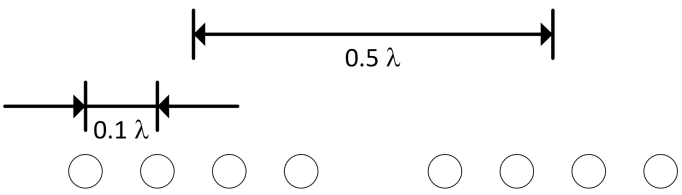

Fig. 8. Array configuration composed of mutually coupled subgroups

C. Calibration Procedure

Principally antenna calibration addresses two different types of calibration procedures for different purposes. The first type, single direction calibration, is considered for TX and RX on multiple antenna equipment. It is used to control timing alignment and amplitude offset of different antenna ports. In LTE less than 65ns among multiple antenna ports has to be guaranteed.
The second type exploits channel reciprocity, particularly in TDD, within the limits of channel coherence time. In order to exploit channel reciprocity, identical TX/RX RF paths are required to get perfect alignment in phase and amplitude. Hence calibration compensates for the mismatch of the baseband-to-RF and RF-to-baseband chains. Actually, since the main purpose of exploiting channel reciprocity is performing adaptive beamforming or non-codebook precoding based on uplink channel sounding (to obtain CSIT), the requirement for calibration is aligning the TX/RX chain response ratio of multiple TX and RX pairs:

$$\frac{\alpha_{1TX}}{\alpha_{1RX}} = \frac{\alpha_{2TX}}{\alpha_{2RX}} = ... \frac{\alpha_{nTX}}{\alpha_{nRX}} \quad \forall n = 1, ..., N \tag{3}$$

where $\alpha_{nTX/RX}$ is the response of the n-th TX/RX RF chain. Based on traditional self-calibration approach, the authors propose over-the-air (OTA) calibration based solution for mMIMO arrays that require only air interface information exchange for AP(access point)-to-AP or AP-to-UE. More specifically, AP1 could be calibrated with the assistance of AP0, assuming that AP0 has been calibrated already. OTA based calibration may not be limited to single AP to AP and can be extended to cluster of APs in network MIMO. Inheriting LTE network listening based synchronization, one straightforward approach

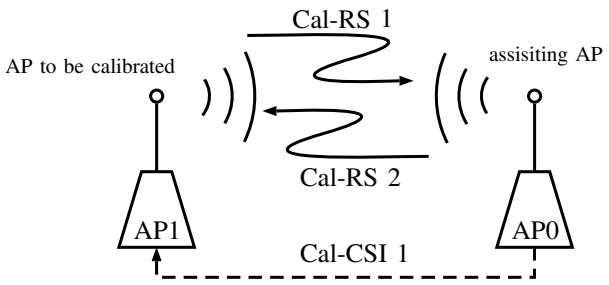

Fig. 9. OTA calibration procedure between 2 APs

is that one AP listens to another AP calibration reference signal, where each AP is assigned with one specific stratum level. Upon this stratum by stratum spreading, the complete network can be fully calibrated.

D. ADC Performance Predictions for 2020

In current commercial LTE UEs (UE category class 6) the maximum bandwidth (BW) is 40MHz, implemented using two 20MHz bands in a Carrier Aggregation configuration. The resolution of such an LTE ADC is estimated to be 12 effective number of bits (ENOB) because it needs to support higher order modulation, use of advanced receivers and the large dynamic range of the received signal. In 2020 the same ENOB is expected, but the bandwidth needs to be at least 100MHz per component carrier (CC). In the following it is discussed if the ADC bandwidth enlargement is achievable with reasonable power consumption.

A good starting point to predict ADC performance in 2020 is to examine how the cellular bandwidth has improved from 2G (200kHz) to LTE (20MHz) over ≈20 years, which is $10^{\frac{\log_{10}(100)}{20\text{ years}}} - 1 = 26\frac{\%}{\text{year}}$. In previous work Manganaro [16] estimated the energy efficiency for high speed ADCs (2BW≥100 MHz) to improve 1.82 dB/year, while high resolution ADCs (signal to noise and distortion ratio SNDR≥75 dB) only improve 0.8dB/year. In 2010 Jonsson [17] conservatively estimated that the ADC peak sampling rate would increase less than 5 times until 2020, but in 2013 his collection of data [18] shows that the thermal Figure-of-Merit (FOM) improves 10 times every decade. In a recent discussion with Stacy Ho of Mediatek, he predicted the Schreier FOM may improve 10dB from 2014 to 2020. Assuming the predicted performance improvement is solely used for BW enlargement (keeping power consumption and ENOB constant) Fig. 10 shows that a 100MHz BW is possible in 2020. The average value is in line with the generally accepted 25-40 % technology factor improvement per year. The ADC power consumption in 2020 can be estimated by updating the Schreier FOM, which is defined as

$$\text{FOM}_\text{S} = \text{DR} + 10\log_{10}(\text{BW}/\text{P}) \quad (4)$$

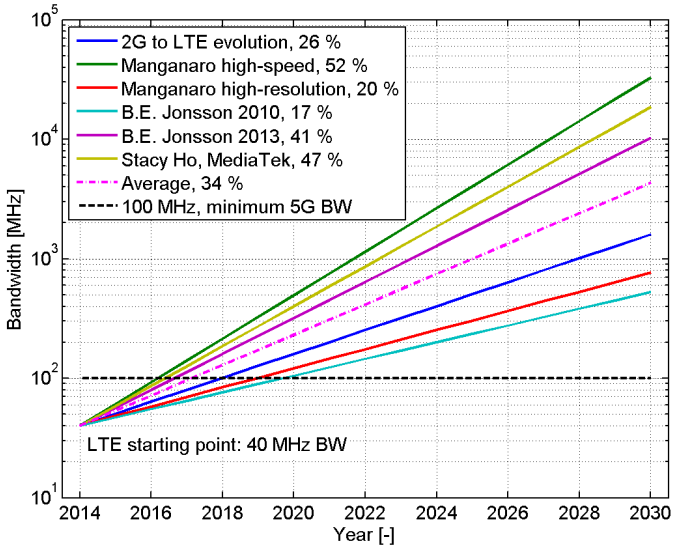

Fig. 10. Predicted ADC BW assuming constant power consumption and ENOB

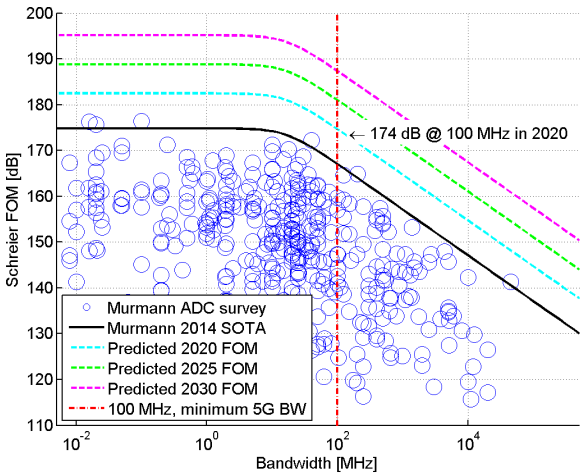

Fig. 11. Murmann state-of-the-art ADC survey [19] combined with predicted Schreier FOM improvement from Fig. 10

where DR is the dynamic range and P is the power consumption. Figure 11 shows the FOM_S plotted using Murmann's data [19] and the estimated average improvement of $34\,\% \rightarrow 1.34^{(2020-2014)} = 7.6\,\text{dB}$. Currently the FOM is about 167dB for a 100MHz ADC, which assumes 12 ENOB corresponds to $\text{DR} = 6.02 \cdot \text{ENOB} + 1.76 = 74\text{dB}$ and entails a power consumption of

$$\text{P}_{100} = \frac{\text{BW}}{10^{(\text{FOM}_\text{S}-\text{DR})/10}} = \frac{100\,\text{MHz}}{10^{(167-74)\text{dB}/10}} \approx 50\,\text{mW} \quad (5)$$

Using eq. (5) and the predicted FOM_S of 174dB the power consumption in 2020 will be P_{100} ≈10mW. Based on a constant FOM_S a doubling of the BW will entail the double power, but since Murmann [19] has also assumed the FOM_S slope to be -10dB/decade, the power consumption in 2020 as a function of bandwidth is estimated to be:

$$P_\text{BW} = \text{P}_{100} \cdot \left(\frac{\text{BW}\ [\text{MHz}]}{100\,\text{MHz}}\right)^2\Bigg|_{\text{BW}=200\text{MHz}} = 40\,\text{mW} \quad (6)$$

Note that some combinations of BW, ENOB and P may not be feasible due to technical constraints, even though the FOM_S is realistic, but for now the scaling in eq. (6) is used. Obviously a narrowband ADC consumes less power than a wideband ADC, but if a certain bandwidth is needed to achieve a specific throughput, the question is whether it is more efficient to use one wideband ADC or multiple narrowband ADCs. The latter option may take up more physical space and furthermore it also necessitates multiple radio frequency front-ends. This is also the case when the number of spatial layers is increased. Note that we do not model possible power savings of combining multiple ADCs in one IC to share voltage reference source, digital control and so forth. To calculate the total power consumption the RF power model from [20] is used, covering both the I and Q branch and includes the power consumption of the low noise amplifier, mixers, the shared voltage controlled oscillator and other phase locked loops components, variable gain amplifiers and analog baseband filters. The power is a function of noise figure and third order intercept point performance, because the components in general are not considered BW dependent. At medium performance the estimated power in 2013 is 9.8mW, which in

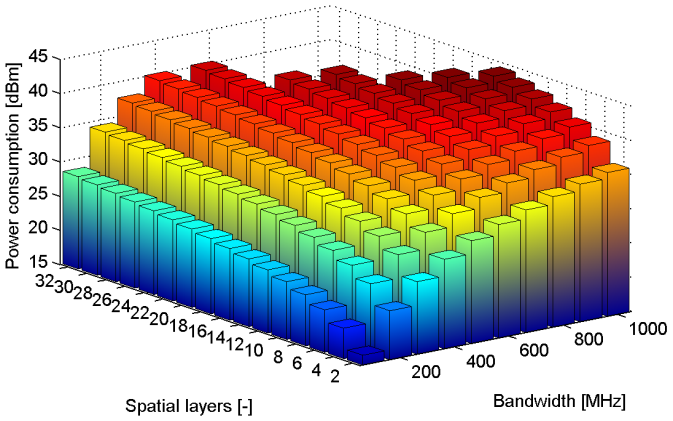

Fig. 12. ADC and RF power consumption in dBm as a function of BW and number of spatial layers.

TABLE IV. ADC AND RF POWER CONSUMPTION AS A FUNCTION OF BW, NUMBER OF SPATIAL LAYERS, AND NUMBER OF CCS.

ADC	RF	Scaled to 1 GHz				
(and CC) BW	chain power	# of carriers	1 spatial layer # ADCs	Power	2 spatial layers # ADCs	Power
100 MHz	22.1 mW	10	20	221 mW	40	441 mW
200 MHz	82.1 mW	5	10	410 mW	20	821 mW
500 MHz	502 mW	2	4	1.00 W	8	2.00 W
1000 MHz	2.00 W	1	2	2.00 W	4	4.00 W

2020 is scaled to $9.8\,\mathrm{mW}/1.25^{(2020-2013)} = 2.06\,\mathrm{mW}$. Figure 12 shows the power consumption for various combinations of 5G BW and spatial layers, and as expected the power consumption increases with both parameters. If the target bandwidth is e.g. 1GHz it can be achieved by the use of multiple CCs, where each CC has a smaller bandwidth hence also less strict ADC performance requirements. Table IVshows the power consumption for various CC BWs. Because the power consumption depends quadratic on the bandwidth, the 100MHz case is the best solution from a power consumption perspective, but it will entail a major increase in chip area to implement 10 CCs.

IV. CONCLUSION

Massive MIMO is widely considered as one key enabler for filling the capacity gap towards the next generation mobile communications. A crucial prerequisite for successful massive MIMO integration into 5G is to scale the total cost for the individual antenna element down by the same factor as the number of antenna elements is increased. Based on that condition various deployment scenarios and implementation concepts have been analyzed. For the 3GPP office scenario a single large scale antenna array at a central TX location has been contrasted with distributed arrays excluding and including cooperation. Furthermore various implementation aspects of the large scale array such as mutual coupling of subgroups for tight arrangement of antennas, calibration issues and estimated ADC performance in 2020 have been investigated. The discussion highlighted relevant aspects for realizing inexpensive massive MIMO solutions for 5G at 2020 time-scale.

ACKNOWLEDGMENT

Stefan Dierks is supported by the German Ministry of Education and Research in the framework of an Alexander von Humboldt Professorship. Mads Lauridsen is partly funded by the Danish National Advanced Technology Foundation and the 4GMCT Project.

REFERENCES

[1] T. L. Marzetta, "Noncooperative cellular wireless with unlimited number of base station antennas," *IEEE Trans. Wireless Commun.*, vol. 9, no. 11, pp. 3590–3600, Nov. 2010.

[2] D. Gesbert, M. Kountouris, R. W. Heath., C.-B. Chae, and T. Sälzer, "Shifting the mimo paradigm," *IEEE Signal Process. Mag.*, vol. 24, no. 5, pp. 36–46, Sept. 2007.

[3] E. G. Larsson, O. Edfors, F. Tufvesson, and T. L. Marzetta, "Massive mimo for next generation wireless systems," *IEEE Commun. Mag.*, vol. 52, no. 2, pp. 186–195, Feb. 2014.

[4] F. Rusek, D. Persson, B. K. Lau, E. G. Larsson, T. L. Marzetta, O. Edfors, and F. Tufvesson, "Scaling up mimo - opportunities and challenges with very large arrays," *IEEE Signal Process. Mag.*, vol. 30, no. 1, pp. 40–60, Jan. 2013.

[5] Nokia Solutions and Networks, "Technology Vision 2020 Whitepaper," pp. 1–16, 2013.

[6] J. Zhang and G. de la Roche, Eds., *Femtocells: Technologies and Deployment*. Wiley, 2013.

[7] 3GPP, "TR36.814 - Further advancements for E-UTRA physical layer aspects," Tech. Rep. v9.0.0, Mar. 2010.

[8] P. Kyösti, J. Meinilä, and L. Hentilä, "Simulation WINNER II D1.1.2 v.1.1: WINNER II channel models," WINNER, Tech. Rep., 2007.

[9] S. Jaeckel, L. Raschkowski, K. Borner, and L. Thiele, "Quadriga: A 3-d multi-cell channel model with time evolution for enabling virtual field trials," *IEEE Trans. Antennas Propag.*, vol. 62, no. 6, pp. 3242–3256, June 2014.

[10] A. Wiesel, Y. C. Eldar, and S. Shamai, "Zero-forcing precoding and generalized inverses," *IEEE Trans. Signal Process.*, vol. 56, no. 9, pp. 4409–4418, Sept. 2008.

[11] P. Mogensen, K. Pajukoski, E. Tiirola, E. Lähetkangas, J. Vihriälä, S. Vesterinen, M. Laitila, G. Berardinelli, G. W. O. D. Costa, L. G. U. Garcia, F. M. L. Tavares, and A. F. Cattoni, "5G Small Cell Optimized Radio Design," in *GlobeCom Workshops*, Atlanta, Dec. 09-13 2013, pp. 111–116.

[12] X. Zhang and J. Lee, "Low complexity mimo scheduling with channel decomposition using capacity upperbound," *IEEE Trans. Commun.*, vol. 56, no. 6, pp. 871–876, June 2008.

[13] J. D. Boerman and J. T. Bernhard, "Performance study of pattern reconfigurable antennas in mimo communications systems," *IEEE Trans. Antennas Propag.*, vol. 56, no. 1, pp. 231–236, Jan. 2008.

[14] V. Jungnickel, V. Pohl, and C. von Helmolt, "Capacity of mimo systems with closely spaced antennas," *IEEE Communication Letters*, vol. 7, no. 8, pp. 361–363, Aug. 2003.

[15] S. Dumanli, C. Railton, and D. Paul, "Decorrelation of a closely spaced antenna array and its influence on mimo channel capacity," in *European Conference on Antennas and Propagation*, Edinburgh, Nov. 11-13 2007.

[16] G. Manganaro, "Advanced Data Converters," in *Cambridge University Press*, 2012.

[17] B. Jonsson, "A survey of A/D-Converter performance evolution," in *17th IEEE conference on Electronics, Circuits, and Systems*, Athens, Dec. 12-15 2010.

[18] ——, "A/D-converter performance evolution v.1.1," www.admsdesign.com, 2013.

[19] B. Murmann, "ADC Performance Survey 1997-2014," http://www.stanford.edu/m̃urmann/adcsurvey.html, 2014.

[20] A. Didioui, C. Bernier, D. Morche, and O. Sentieys, "Power reconfigurable receiver model for energy-aware applications," in *IEEE 56th International MWSCAS*, Columbus, Aug. 4-7 2013.